Physics of Electron Beam Ion Traps and Sources

Fred Currell and Gerd Fussmann

Invited Paper

***Abstract*—This paper presents the basic physics underlying the operation of electron beam ion traps and sources, with the machine physics underlying their operation being described in some detail. Predictions arising from this description are compared with some diagnostic measurements.**

***Index Terms*—Electron beam ion source (EBIS), electron beam ion source/trap (EBIS/T), electron beam ion trap (EBIT), ion source, ion trap.**

I. Introduction

ELECTRON beam ion sources and traps (EBIS/Ts) are the table-top devices of choice for those wanting to create and study highly charged ions. An EBIS/T uses a magnetically compressed, quasi-monoenergetic high energy and high current density electron beam to sequentially ionize atoms or ions with a low charge state. The long confinement time required for the stepwise ionization is achieved by keeping the ions in an ultra-high vacuum trapping environment whilst exposing them to the electron beam. Radial trapping is achieved through the space charge of the electron beam, axial trapping by the negative biasing of a central drift tube with respect to two end drift tubes. If a low background pressure is not achieved, background gas rapidly becomes ionized and trapped. These ions in turn neutralize the electron beam's space charge, preventing the radial trapping from working properly and hence, limiting the charge states which can be obtained. This phenomenon is called *compensation*.

To achieve a sufficiently high ionization rate, the electron beam is magnetically compressed whilst being accelerated electrostatically to the required energy (ranging typically from 500 eV to 200 keV). This beam is launched from a high perveance electron gun sited in a region of zero or low magnetic field. From here, it is accelerated toward the trap region, being compressed by a rising magnetic field, which reaches its peak value at the trap region. This magnetic field is created using either a single solenoid or a pair of superconducting Helmholtz coils, situated around the trap region.

In contrast to other types of ion sources (e.g., electron cyclotron resonance ion source, ECRIS) which also make use of electron impact ionization, the quasi-monoenergetic nature of the electron beam used in EBIS/Ts has the particular benefit that the trapped ions are not exposed to low energy electrons. The electron–ion recombination cross section scales approximately as $1/E_e$ where E_e is the interaction energy. Hence, low energy electrons give rise to a large recombination rate, tending to drive the charge balance in other ionization sources toward lower charge state. Futhermore, control of this electron beam energy allows one to preferentially create a few selected charge states, particularly at or near closed shell configurations.

The electron beam ion source (EBIS) was first developed by Donets *et al.* [1], [2]. Previous to the development of this device, the concept had been used, although not with nearly the same degree of success. Furthermore, previous devices lacked many of the refinements introduced by Donets' group.

Perhaps the earliest use of the principle that a magnetically compressed electron beam interacting with atoms can produce positively charged ions dates back to Bleakney in 1929 [3]. Subsequently, Plumlee [4] used an ion trap in the source of a mass spectrometer and observed positive ions of mercury up to Hg^{5+}. Collision processes were first studied by Baker and Hasted [5] who measured ionization cross sections for Ne^{+}, Ar^{+}, Kr^{+}, and Xe^{+}. Trapping was provided by the space charge of a magnetically confined electron beam and confinement times of around 100 μs were achieved. Redhead [6] improved the axial trapping by adding potential barriers at the ends of the ionization region. The improved trapping, with trapping times of up to 0.5 s and the use of higher electron densities lead to ions with charge states up to Ar^{6+}, Kr^{7+}, and Xe^{10+} being observed.

Following related developmental work by Schmieder *et al.* [7], the first electron beam ion trap (EBIT) was developed by Levine *et al.* [8]. EBITs have a Helmholtz coils arrangement to allow radiation to enter and leave the trap region through observation ports. Hence, they can be used for spectroscopy. They are also generally constructed with a short trap length (typically 3 cm) to ensure certain plasma instablities do not occur [9]. However, more recent developments [10] suggest that this restriction can be relaxed.

The original EBIT was upgraded for higher energy operation, being dubbed super-EBIT [11]. Among the range of notable achievements made with the upgraded device was the creation of bare uranium [12]. With this important milestone, EBIT technology came of age, demonstrating that any ion of any stable element can in principle be created and studied with these machines or delivered to other apparatus.

In literature, there has often been a distinction made between EBISs and EBITs. EBISs, as their name implies, are used to de-

Manuscript received May 22, 2005; revised July 17, 2005.

F. Currell is with the Department of Physics and Astronomy, School of Mathematics and Physics, Queen's University of Belfast, Belfast BT7 1NN, Northern Ireland, U.K. (e-mail: f.j.currell@qub.ac.uk).

G. Fussmann is with the Institute for Physics, Humboldt-Universität zu Berlin, 12489 Berlin, Germany (e-mail: gerd.fussmann@physik.hu-berlin.de).

Digital Object Identifier 10.1109/TPS.2005.860072

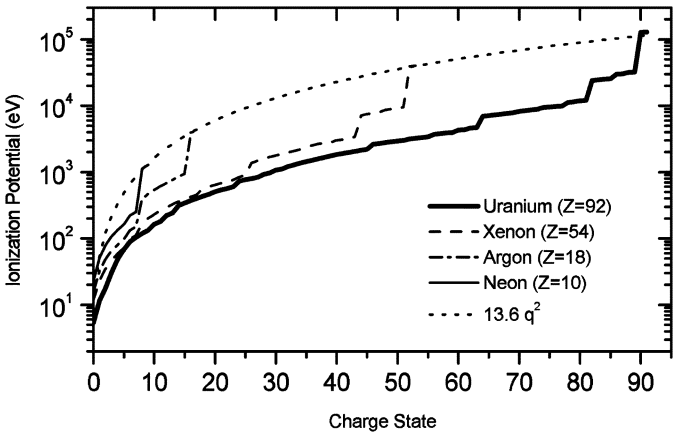

Fig. 1. Ionization potential plotted as a function of charge state for selected elements. Data from [14].

liver ions to other experiments while EBITs exploit the split solenoid arrangement for detection and introduction of photons for *in situ* studies. However, this distinction is somewhat arbitrary since most EBITs are used to deliver ions to other experiments and the underlying machine physics is essentially the same. Accordingly, throughout this paper, we will generally use the term, EBIS/T, except where specific differentiation is required.

The community of EBIS/T users enjoys a (typically) biennial conference specifically devoted to these devices and their applications. The most recent, the "Ninth International Symposium on Electron Beam Ion Sources and Traps and Their Applications (EBIS/T 2004)" was held at Tokyo Metropolitan University, Tokyo, Japan. The proceedings of this meeting provide an up to date summary of developments in the field [13].

Since EBIS/Ts achieve ion creation through electron impact ionization, and since the ionization potential grows rapidly with increasing nuclear charge (becoming as high as 137 keV for the final electron orbiting hydrogen-like uranium), a high energy electron beam is required. Fig. 1 shows the ionization potential as a function of the charge state being ionized for selected elements. Additionally, the $13.6q^2$ limit for creation of bare ions is also shown. In practice, one requires an EBIS/T to be operating at two or three times the ionization potential of the ion of charge $q-1$, where q is the required charge state. This is done to ensure sufficient creation since the ionization cross section slowly increases from the threshold.

In the trap region of an EBIT, a wide array of processes occurs as is illustrated schematically in Fig. 2. An ion interacting with the electron beam can be stripped of one or more of its electrons through electron impact ionization, driving it up the staircase shown. Recombination reactions can occur, whereby an ion can gain an electron, emitting one or more photons of characteristic energy to stabilize the ion, resulting in the ion moving one step down the staircase. Even in the best vacuum there is some residual gas. Being very highly charged, the trapped ions have a large cross section for charge exchange, the predominant process resulting in the transfer of a single electron. This again will move the ion one step down the staircase. As is described in Section II, it is usually possible to ascribe a temperature to each charge state of the trapped ions. Since the ions are trapped with a finite trapping depth, ions from the high velocity tail of

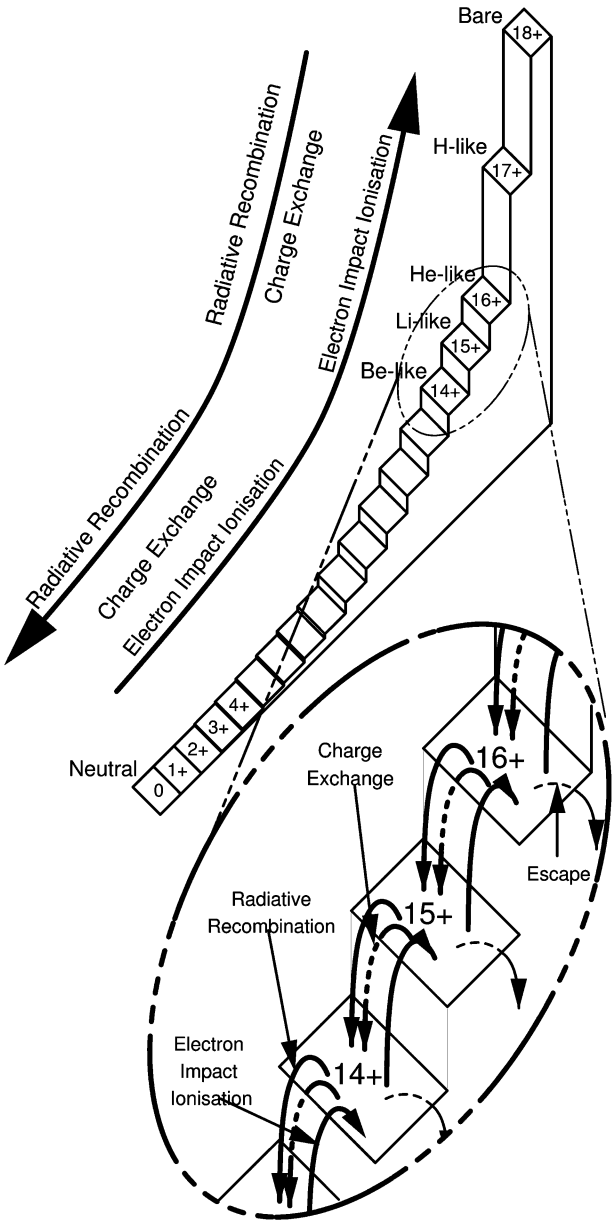

Fig. 2. Schematic representation of the coupling of neighboring charge states of Ar ions due to atomic physics processes. Height of each step is proportional to the ionization potential required to form that charge state to emphasize the increased difficulty in creating the higher charge states. Insert shows the couplings between neighboring charge states and the escape process.

the velocity distribution associated with a given charge state are able to escape from the trap. All of these "charge changing" and escape processes typically occur on time scales of the order of 10 ms.

The motion of a single ion in the EBIS/T trapping environment occurs on a much quicker timescale and is amenable to an analytical description [15]–[17]. However, this description is not particularly valuable toward understanding the charge evolution of ions in an EBIS/T. At the ion densities and temperatures typically encountered in EBIS/Ts, ion–ion collisions lead to cross-field diffusion on a time scale faster than the charge changing and escape processes depicted in Fig. 2. This cross-field diffusion causes the trapped ions to form a cloud, which surrounds and penetrates the electron beam, with the highest

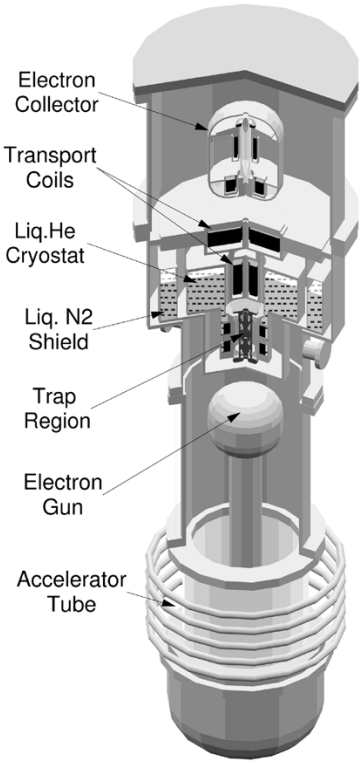

Fig. 3. Schematic figure of the Tokyo EBIT. Note, the collector support and associated accelerator tube are not shown. Magnetic coils are shown as the darkest regions of the figure.

density along the electron beam axis. Once cross-field diffusion is considered within the framework of the Vlasov equation [15] or otherwise [16], it can be shown that the magnetic field no longer plays any role in long-term trapping of the ions. The description of ion trapping then can be made in terms of the electrostatic potential of the system alone. Such a description is outlined in Section II-B.

In order to properly determine the electrostatic potential, one must start with a description of the electron beam. Such a description is given after the main component parts of an EBIT are outlined in Section II. Section II-C describes the dynamics of forming the charge balance of trapped ions inside an EBIS/T. Since the spatial distribution of the ions of a given species is determined by its characteristic temperature, the temperature dynamics is discussed in Section II-D. The result is a self-consistent but somewhat complicated description of the machine physics of EBIS/Ts. Through various approximations, a considerably simpler, but also considerably more approximate description of the ion creation rate for a given species and set of machine parameters is developed. The more complete description is compared to various machine physics related experiments in Section III through which the model is essentially validated.

II. Machine Physics

The major subassemblies of an EBIS/T, the electron gun, the trap and the collector all lie along a single beam axis, as is illustrated in Fig. 3. The trap region is surrounded by magnetic coils and consists of a series of cylindrical drift tubes through which the electron beam passes. In several machines, the magnetic coils are super-conducting, being held typically at a temperature of around 4 K by liquid helium. The drift tubes are in good thermal contact with the cryostat, so they are cooled to a similar temperature, acting as an efficient cryopump for the trap region. The electron gun is designed to produce a high current laminar flow electron beam suitable for acceleration into the trap region. The outside of the electron gun is encased in soft iron, to shield the cathode from the magnetic field due to the superconducting magnet. Launching the electron beam from a region of zero or near zero magnetic field ensures maximum beam compression. It is important that the magnetic field rises in the correct manner to ensure the compression occurs without significant scalloping of the electron beam. This condition is usually ensured through trajectory simulations using well-established software packages [18], [19].

Typically, the electron beam can have a current of 100 mA and have been accelerated through a potential of 30 kV. Hence, to dump it would require dissipation of 3 kW of direct current power. Clearly, this is unreasonable so instead the electron beam is decelerated as it moves toward a collector assembly also situated in a region of zero or low magnetic field. The electron beam enters the collector, expanding due to the reducing magnetic field, and is finally collected on the inner face of the collector electrode which is biased typically 1 kV positive with respect to the cathode. Just in front of the electrode used to collect the electrons are one or more suppressor electrodes. These act to stop low energy secondary electrons from leaving the collector. Otherwise, these electrons could be re-accelerated back along the beam axis to subsequently collide with parts of the trap region.

In the following description of the physics occurring in the trap region of such a machine, the generic label i will be used to refer to a particular charge state of ions as an index. Properly we should also use a second subscript α to denote the particular element trapped in the EBIS/T as it is quite common to operate EBIS/Ts with ions of more than one element being trapped. Hence, there is a unique value of i and α for each species trapped. For example, the number density of charge state i of element α should be denoted $n_{i,\alpha}$. In most cases, in this account, we drop the index α throughout for brevity. However, when denoting the index to summations, a double index i, α or j, α will be used when the summation is over all charge states of all elements. For readability, we denote the charge number by $\hat{q}_i$ where it is not being used as an index, and use q_i for the charge of the ion. Hence, $q_i = e \times i = e \times \hat{q}_i$ where e is the elementary charge.

Several assumptions are usually made when describing the machine physics of EBIS/Ts. These assumptions are that there is cylindrical symmetry of the trap environment, there is a square shaped axial potential and that each charge state of trapped ions has a single temperature applicable to all degrees of freedom. However, a distinct temperature must be associated with each charge state, with the higher charge states having higher temperatures. Each of these assumptions is reasonable, as will be shown below. One more assumption commonly made is that both the trap and the ion distributions are much longer than they are wide. In EBITs, with their characteristically shorter trap regions, this final assumption is valid only when the depth of the axial potential is less than about 150 V [17].

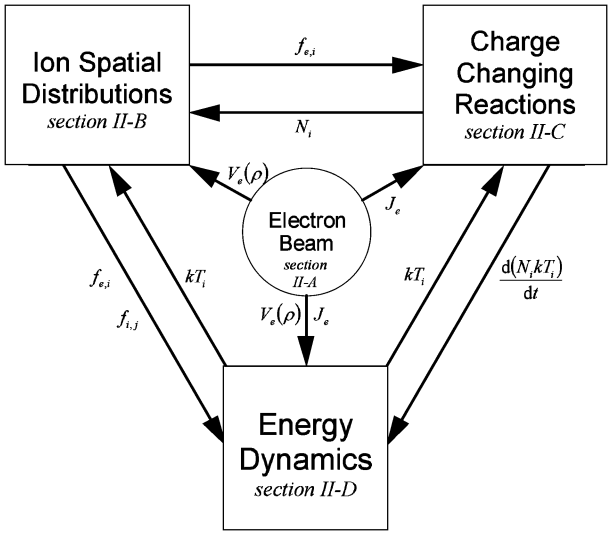

Fig. 4. Summary of relationships in the machine physics of EBIS/Ts and the sections in this paper in which they are described. Arrows show causal links with the corresponding variables being shown alongside the arrows. $f_{e,i}$ and $f_{i,j}$ are overlap factors which serve to scale various interactions according to the overlap of the species concerned. N_i is the number density on axis per unit length of the trapped species and T_i is its temperature. $V_e(\rho)$ is the space charge potential of the electron beam and J_e is its current density.

There are several inter-related concepts underlying the machine physics as are summarized in Fig. 4. With the exception of charge exchange, the *electron beam* drives all the atomic physics processes occurring in the trap (see Fig. 2). It also provides radial trapping and hence determines the spatial distribution of the trapped ions through $V_e(\rho)$. Through the Landau–Spitzer and ionization heating mechanisms described below, the electron beam also heats the trapped ions.

Charge dynamics refers to processes which lead to trapped ions being created or changing their charge state through atomic physics reactions or escaping (axially or radially) from the trap. Axial number densities (N_i) can be used to track this dynamics, providing normalization factors for the spatial distributions.

Energy dynamics refers to processes which change the characteristic temperature (kT_i) associated with a particular species. The units of temperature used throughout this paper are electronvolts as temperatures are often compared to some form of electrostatic potential experienced by the ions. Hotter ions spend less of their time close to the beam axis and hence have lower electron–ion overlap factors, $f_{e,i}$. The electron beam provides the major source of heating, having the biggest effect on higher charge states. Cooling is predominantly made through axial escape, which happens faster for higher kT_i and lower charge states. Ion–ion collisions give rise to energy sharing between the different charge states meaning that while distinct temperatures are required for the various charge states, they vary smoothly across the range of charge states. Because the heating happens most strongly for higher charge states while the cooling is predominantly of the lower charge states, the temperature tends to increase as the charge state increases. However, when considering the trapping of the ions, the important factor is the ratio of the temperature to the potential experienced by the ions including its charge state i.e., terms like $q_i V/kT_i$. This term increases as the charge state increases and so the higher charge states tend to be more strongly trapped, which is a very important property of EBIS/T operation.

Ion spatial distributions (one per charge state) describe the locations of trapped ions. These can be most conveniently cast as axial number densities per unit length by assuming the ion cloud is much longer than it is wide. These distributions generally extend beyond the electron beam and ions explore the whole phase space available to them faster than charge-changing or escape processes occur. Hence, it is meaningful to derive overlap factors between ion species i and the electron beam $(f_{e,i})$ or ion species j $(f_{i,j})$ and to use these overlap factors to scale the rates of various processes which lead to change of charge or energy or both. Work must be done to change the spatial distributions since it requires transport of ions across equipotential contours. This work is accounted for within the framework of the energy dynamics.

A. The Electron Beam

A zero-temperature electron gas correctly launched from a cathode situated at zero magnetic field would be expected to be compressed by a magnetic field of B to form a beam with a characteristic radius equal to the Brillion radius

$$r_b[\mu\mathrm{m}] = \frac{150}{B[T]}\sqrt{\frac{I_e[A]}{\sqrt{E_e[\mathrm{keV}]}}} \tag{1}$$

where I_e is the electron current in the beam, and E_e is the electron beam energy at the trap, with the dimensions of the quantities being given in square brackets. Since the electrons are emitted thermionically, they have a nonzero temperature so (1) provides an overestimate of the compression achieved. In such a situation, Herrmann theory [20] gives a good prediction for the measured radius [21]–[23] through which 80% of the beam passes as

$$r_h = r_b\sqrt{\frac{1}{2}+\frac{1}{2}\sqrt{1+4\left(\frac{8kT_c r_c^2 m}{e^2 r_b^4 B^2}+\frac{B_c^2 r_c^4}{B^2 r_b^4}\right)}}. \tag{2}$$

Here, r_c is the cathode radius, kT_c is the characteristic electron energy at the cathode, m is the electron mass, e is the proton charge, and B_c is the magnetic field at the cathode. The beam radius becomes a minimum when $B_c = 0$. This is the reason EBIS/Ts have the soft iron shield and bucking coil described above. In practice, the bucking coil current is usually empirically tuned for best performance in terms of extracted ion yield or detected photon yield (EBITs only) rather than the actual beam radius being measured. Provided the ratios in round brackets are dimensionless, any system of units can be used for the quantities in (2), with r_h and r_b having the same units. For example, if SI units are used for all the other quantities and r_b is taken from (1), then r_h has units of micrometers. The first term in round brackets is usually much greater than unity. Neglecting the comparatively small constants, enforcing $B_c = 0$ and converting to suitable units, the minimum attainable beam radius is then

$$\begin{aligned} r_h &= \left(\frac{8m}{e^2}kT_c\right)^{1/4}\sqrt{\frac{r_c}{B}} \\ &\approx 2.59\times 10^{-3} T_c^{1/4}\sqrt{\frac{r_c}{B}} \end{aligned} \tag{3}$$

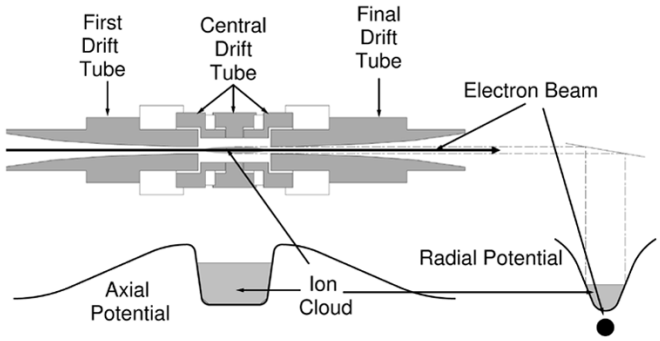

Fig. 5. Schematic figure of the trapping environment of the Tokyo EBIT. Insulators are shown by the white regions of the figure; metal by the dark regions. The whole trap has cylindrical symmetry. Usually the three central metal electrode are shorted to act as a single drift tube.

with T_c in electronvolts and all other quantities in SI-units. This equation predicts a beam radius of about 30 μm, consistent with several measurements for the machines concerned [21]–[23].

Assuming the electron beam has a "top-hat" like profile with all the charge bounded inside a radial region r_e (typically about equal to the Herrmann radius r_h) lying along the axis of cylindrical symmetry of the machine, the potential is given by Poisson's equation to be

$$V_e(\rho) = V_0 \left(\frac{\rho}{r_e}\right)^2 \text{ if } \rho < r_e \tag{4}$$

$$V_e(\rho) = V_0 \left(2\ln\left(\frac{\rho}{r_e}\right) + 1\right) \text{ if } \rho > r_e. \tag{5}$$

Here, V_0 is determined by the total charge per unit length of the electron beam and is given (in convenient units, denoted in square brackets) by

$$V_0[V] = \frac{30I[A]}{\sqrt{1 - \left(\frac{E_e[\text{keV}]}{511} + 1\right)^{-2}}} \tag{6}$$

where $I[A]$ is the total beam current and $E_e[\text{keV}]$ is the electron beam energy. Since V_0 does not depend on the electron beam radius, neither does the potential energy required to move an ion from the centre of the beam to the edge. The form of (5), however, is such that the potential required for an ion to reach the drift tube wall (typically situated 5 mm from the beam axis) does depend on the electron beam radius.

B. Trapping and the Ion Cloud Shape

The essentials of the trapping environment are shown in Fig. 5. It is convenient to treat the trapping potential as separable into the product of radial and axial functions. Although an approximation, this separation is reasonable because the electron beam and the ion clouds are usually much longer than they are wide. Then, the axial distribution is governed largely by the voltages applied to the electrodes whilst the radial distribution is governed by the electron beam's space charge.

The ions are trapped axially by applying suitable voltages to a series of cylindrical drift tubes comprising the trap. Variations in the specific drift tube structure occur from device to device but the conventional mode of operation is where the central drift tube (comprised of three separate electrodes in Fig. 5) is negatively biased by a few volts to a few hundred volts with respect to the outer drift tubes. Radial trapping is due to the electron beam's space charge potential as given by (4) and (5). Axial trapping occurs for all positive ions with a sufficiently low enough axial component of momentum to be "reflected" between the two drift-tube potentials. If a voltage V_{app} is applied to the outer drift tubes with respect to the central drift tube, the trap depth is approximately given by

$$V_t \approx V_{\text{app}} + (V_e(r_{1,3}) - V_e(r_2)) \tag{7}$$

where $r_{1,3}$ is the radius of the inner wall of the two end drift tubes and r_2 is the same quantity for the central drift tube. The second term is a small correction due to the image charge which the electron beam induces on the drift tube walls. The drift-tubes are deliberately shaped so as to produce a nearly square-shaped potential along the beam axis. This distribution has several advantages, including the minimization of ionization heating (see Section II-D). This form of axial potential distribution means that the ion distribution can be considered to be uniform in the space between the two end drift tubes. The depth of this axial potential determines the rate of axial escape of the ions and hence controls the predominant cooling mechanism, discussed in Section II-D.

The trap can be configured with voltages applied asymmetrically (i.e., different voltages applied to the first and last drift tubes with respect to the central drift tube). In this case the lowest of the two V_t values is the one which determines the trap depth. This is because ions make many passes along the trap between collisions and so can find this minimum barrier if they have sufficient axial kinetic energy. This effect can be used to advantage when extracting ions in "leaky mode" (i.e., letting them escape continuously). In such a situation it is usual to bias the drift tube nearest to the collector less than the one nearest to the gun (both with respect to the central drift tube). Then ions preferentially escape toward the collector with a chance of being extracted into the ion transport system.

Since only electrostatic terms have an effect [15], [16], the equilibrium spatial density distribution of the ions of charge q_i and characteristic temperature kT_i is given by a Boltzman distribution

$$n_i(\rho) = n_i(0)e^{-(q_i V(\rho)/kT_i)} \tag{8}$$

where $V(\rho)$ is the electrostatic trapping potential given by

$$V(\rho) = V_e(\rho) + \sum_{i,\alpha} V_i(\rho) \tag{9}$$

$n_i(0)$ is the density of ions of species i, on the beam axis, $\rho = 0$. Note here the summation is over the double index i, α to emphasize it is over all trapped ions. The contribution due to the electron beam, given by $V_e(\rho)$ (4)–(6) is partially compensated for by the sum of $V_i(\rho)$ terms. $V_i(\rho)$ is the potential due to the space charge of ions of charge state i in the trap. $V(\rho)$ must now satisfy Poisson's equation [16]

$$\frac{1}{\rho}\frac{\partial}{\partial\rho}\left(\rho\frac{\partial V(\rho)}{\partial\rho}\right) = \Theta(r_e - \rho)\left(\frac{4V_0}{r_e^2}\right) - \frac{1}{\varepsilon_0}\sum_i q_i n_i(0)\exp\left(-\frac{q_i V(\rho)}{kT_i}\right) \tag{10}$$

with $\varepsilon_0 = 8.85 \times 10^{-12}$ As/Vm. The unit step function $\Theta(r_e - \rho)$ is unity inside and zero outside the electron beam and describes the top-hat shaped charge distribution. Other forms of electron beam profile can be modeled by changing this term. For other realistic beam profiles (e.g., Gaussian) the results are similar to those reported here.

For given sets of n_i and kT_i (10) can be solved for $V(\rho)$ numerically as an initial value problem in two variables, $V(\rho)$ and $(\partial V(\rho)/\partial\rho)$. This problem can be solved by starting at the axis $\rho = 0$ with the value of both of these variables set to zero. Once the solution is propagated to the drift tube, all the values of the potential calculated can then be shifted by an additive constant so that the value of the potential at the drift tube radius is equal to the value applied to the central drift tube, as required by the boundary condition. The information used to solve the right hand side of (10) corresponds to the two arrows pointing into the box labeled "Ion Spatial Distributions" in Fig. 4. Once $V(\rho)$ is determined, the ion cloud radial distributions can be calculated from (8). For species i, the total number of ions per length in the trap N_i, and the total number in the beam N_i^{in} are given by the appropriate integrals over the resultant distribution

$$N_i = n_i(0)\int_0^{r_{dt}} 2\pi\rho \exp\left(-\frac{q_i V(\rho)}{kT_i}\right) d\rho \tag{11}$$

and

$$N_i^{in} = n_i(0)\int_0^{r_e} 2\pi\rho \exp\left(-\frac{q_i V(\rho)}{kT_i}\right) d\rho. \tag{12}$$

The electron–ion overlap factor is the ratio of ions inside the electron beam to ions in the trap

$$f_{e,i} = \frac{N_i^{in}}{N_i}. \tag{13}$$

Hotter ions spend less time in the electron beam, have lower electron–ion overlap factors and hence have lower rates for electron–ion interactions. Trapped ions compensate for the space charge of the electron beam which acts to trap them. Eventually, the radial trapping is completely removed when the positive charge of the trapped ions exactly compensates the negative charge of the electron beam. However, if the axial trap depth is shallow enough (typically a few times V_0), the highest charge states are confined inside the electron beam and the space charge of the electron beam is only slightly compensated by the trapped ions.

C. Charge Evolution

The range of processes involved in the charge evolution of ions in an EBIS/T can be represented as a "staircase," as shown in Fig. 2. Because double ionization and charge transfer generally have cross sections at least an order of magnitude less than their single counterparts, these processes can be neglected. Also, the temperature of the trapped ions is sufficiently low that charge exchange only occurs through ion–neutral collisions. The Coulomb barrier prevents a pair of ions coming close enough for charge exchange to occur. Note that the picture is considerably simplified because adjacent charge states are coupled to each other only. Ions can also escape from the trap as is described in Section II-D. For the general case, a series of coupled differential equations, one for each charge state can describe these processes

$$\begin{aligned}\frac{dN_i}{dt} = &\frac{J_e}{e}\left(N_{i-1}\sigma_{i-1}^{EI} f_{e,i-1} - N_i\sigma_i^{EI} f_{e,i}\right)\\ &+ \frac{J_e}{e}\left(N_{i+1}\sigma_{i+1}^{RR} f_{e,i+1} - N_i\sigma_i^{RR} f_{e,i}\right)\\ &+ n_0\left(N_{i+1}\left\langle v\sigma_{i+1}^{CX}\right\rangle - N_i\left\langle v\sigma_i^{CX}\right\rangle\right)\\ &- N_i R_i^{Esc}.\end{aligned} \tag{14}$$

The first line of (14) describes electron impact ionization (EI). There are two terms in brackets, accounting for creation of species i from species $i-1$ (hence, positive sign) and for annihilation of species i along with creation of species $i+1$ (hence, negative sign). Similarly, the second line describes creation and annihilation of species i by radiative recombination (RR). Both, electron impact ionization and radiative recombination are due to interactions with electrons from the electron beam. Hence, the cross sections are functions of the electron beam energy and the corresponding rates scale linearly with the current density $J_e = en_e v_e$.

The electron impact ionization cross section (σ^{EI}) rises from zero at threshold to generally peak at two or three times the ionization potential associated with the reaction. For very highly charged systems, this maximum can occur at higher energy or the cross section might even increase indefinitely due to quantum electrodynamical effects. For measurements of this phenomenon made using EBITs and more details see [24]–[26] and references therein. The electron impact ionization cross section becomes smaller as more electrons are stripped away from the target. i.e., becomes smaller for increasing q_i. In contrast, the radiative recombination cross section (σ^{RR}) scales roughly as q_i^4/E_e. In is noted that the radiative recombination rate scales as $q_i^4/\sqrt{E_e}$ due to the $\sqrt{E_e}$ dependence on J_e through its dependence on the electron velocity.

Suppose one is interested in creating a charge balance dominated by a given charge state. From the energy dependencies described above, it is advantageous to use an electron beam energy several times greater than the threshold required to create the charge state required. However, there is a difficulty that at this energy further stripping of electrons can occur so higher charge states can be made. As is shown in Fig. 1, the ionization potential as a function of charge state shows step-like discontinuities. Each of these discontinuities corresponds to opening a new electron shell or otherwise breaking a particularly stable electron configuration (e.g., nickel-like). In the situation that one wants to make a charge state corresponding to a close shell configuration, one can use these step-like discontinuities by setting the electron beam energy somewhere just below the energy required to open the next shell. Then the ionization cross section for creating the desired charge state is large, the recombination cross section for its annihilation is small and no further ionization can occur. The result is a charge balance strongly peaked at the closed shell configuration. This ability to create a charge balance strongly peaked at a chosen closed shell configuration is the major reason that closed shell highly charged systems are

predominantly used in experiments associated with EBIS/Ts unless a specific electron configuration is required for the science under study. For example, Xe^{44+} is by far the most common highly charged ion extracted from EBIS/Ts for ion-surface interaction studies.

The third line of (14) describes charge exchange (CX) processes. The term scales linearly with the neutral density n_0. Again, there are two terms in brackets to describe creation and annihilation of ions of charge state i. Charge exchange cross sections are averaged over the velocity distribution of ions of species i to give a rate of the form $\langle v\sigma_i^{CX}\rangle$ where v is the relative velocity. The neutral background gas is treated as being uniform and stationary, having a much lower temperature than the trapped ions.

The final term of (14) describes escape from the trap, corresponding to the solid "thin dashed arrows" in Fig. 2. The axial rate of escape of ions is given by [16], [27]

$$R_i^{Esc} = \frac{3}{\sqrt{2}}\nu_i \frac{e^{-\omega_i}}{\omega_i} \tag{15}$$

where $\nu_i = \sum_{j,\alpha} \tau_{i,j}^{-1}$ is the Coulomb collision frequency (see (24) below) for ions of charge state q_i with all ions. Note, this summation is over all trapped ion species so the double index j, α is used in the summation. ω_i is given by

$$\omega_i = \frac{q_i V_t}{kT_i} \tag{16}$$

where V_t [as given by (7)] is the shallowest of the two end axial trap depths over which an ion must pass to escape. These terms describe diffusion in velocity space: due to Coulomb collisions with all ions, a particle performs a random walk in velocity space, but once it passes the axial threshold velocity $v_{\text{thresh}} = \sqrt{(2q_iV_t/m_i)}$ it escapes rapidly from the trap. Note that because $\nu_i \propto n_i$, the last term in (14) contains a sum of double products $\sum_{k,\alpha} N_i N_k$ and thus, introduces a nonlinearity into the otherwise linear system.

An analogous expression to that given in (15) has been derived to describe radial escape [28] but with ω_i replaced by a modified term ω_i^{rad}. The total escape rate is then given by the sum of two terms each of the form of the right hand side of (15), one with ω_i as given by (16) and one with ω_i^{rad} given by

$$\omega_i^{\text{rad}} = \frac{q_i V_{\text{rad}} + q_i B r_{dt}\sqrt{\frac{2kT_i}{3M_i}}}{kT_i}, \tag{17}$$

where V_{rad} is the potential difference (including effects of ion compensation) between the position where the ion is trapped and the central drift tube, B is the magnetic field at the trap, r_{dt} is the drift tube radius, and M_i is the mass of the ion. When $V_{\text{rad}} \gg V_t$, as is often the case, this form of escape tends to be negligible. However, it can become important when V_t is set to be very large (> 100 V) and the electron beam's space charge is almost completely compensated. Indeed, even if the electron beam is switched off, the magnetic field alone can trap the ions for a considerable time through the effect of magnetic trapping alone [29].

In general, charge exchange acts to broaden the charge balance and also move it toward lower charge state. Escape tends to deplete the lower charge states preferentially as ω_i tends to increase as q_i increases. As will be discussed in Section II-D introduction of a lighter system (often Ne or N_2 gas) leads to increased escape of lower charged ions and hence, provides beneficial cooling of the more highly charged ions. This result might at first seem counter intuitive because the increased background gas pressure leads to increased charge exchange. However, this effect is outweighed by the lower temperature of the highly charged ions due to the evaporative cooling by ions of the lighter system being injected.

Equation (14) describes the general case, but special cases exist where some of the terms vanish or require modification. For example, a source term must be included to describe injection of either neutrals or ions of low charge state into the trap. Furthermore, ionization beyond some given charge state might no longer be allowed. In these cases, terms corresponding to creation or annhiliation of energetically forbidden species are simply removed.

There are two limits from which one can derive useful information about EBIS/T behavior, without solving these differential equations exactly, the short-time limit and the equilibrium limit. The short-time limit can be arrived at by supposing the trap is initially empty and then it is suddenly "closed" by raising the outer drift-tube to a potential above the central one. Ions start to accumulate from either a background of neutral gas or some other form of injection. At early times all reactions except ionization can be neglected and the electron–ion overlaps $f_{e,i}$ can be set to one. In this case, the characteristic appearance time for species i is given by

$$t_i^{\text{app}} = \frac{e}{J_e}\sum_{j=1}^{i}\frac{1}{\sigma_j^{EI}} \tag{18}$$

where J_e is the electron current density. This summation is over all the ions of one element, not all ions trapped. In practice, the overlap factors may quickly become less than one and the other reactions may play a role. These effects increase the characteristic appearance time t_i^{app} so (18) provides a lower bound.

The equilibrium limit is arrived at by setting all of the left hand sides of the set of equations represented by (14) to zero. Escape tends to occur predominantly for lower charge states as is outlined in Section II-D, so when considering the high charge states, it too can be neglected and for a low enough value of V_t all ions of the higher charge states tend to be inside the electron beam (i.e., $f_{e,i} \approx 1$). If the trap is constantly filled due to ionization of a background of neutral gas (i.e., the system has a constant source term), then the equilibrium condition can be reached. Provided a sufficiently low neutral gas injection rate is used, the rate for charge exchange is much less than the rate for radiative recombination. Making these assumptions, the equlibrium condition for the highest two charge states of a given trapped substance (the highest charge state being labeled $i_{\max}$)

$$\frac{dN_{i_{\max}}}{dt} = 0 \approx J_e\left(N_{i_{\max}-1}\sigma_{i_{\max}-1}^{EI} - N_{i_{\max}}\sigma_{i_{\max}}^{RR}\right) \tag{19}$$

from which it follows that

$$\frac{N_{i_{\max}-1}}{N_{i_{\max}}} \approx \frac{\sigma_{i_{\max}}^{RR}}{\sigma_{i_{\max}-1}^{EI}}. \tag{20}$$

It can be shown [17] that similar relationships can be derived down the charge staircase, becoming ever more approximate, giving the general result

$$\frac{N_{i-1}}{N_i} \approx \frac{\sigma_i^{RR}}{\sigma_{i-1}^{EI}}. \tag{21}$$

It is emphasized that this result relies on the charge exchange and escape rates being negligible, which may not always be the case. In general, this relationship only applies for a few (the highest) charge states present and even then is an approximation. Checks can be used to ensure these conditions are fulfilled, which is of particular importance when trying to deduce cross sections from the equilibrium behavior of EBITs [25], [26].

D. Energetics of the Trapped Ions

There are several processes involved in determining the temperature dynamics of each trapped ion species. The dominant processes are electron beam heating (sometimes called Landau–Spitzer or Spitzer heating) and evaporative cooling. Electron beam heating occurs through long-range Coulomb collisions taking place between electrons from the beam and trapped ions and has a rate given by

$$\left(\frac{d}{dt}\frac{3}{2}N_i kT_i\right)^{\text{Beam}} = f_{e,i}N_i\frac{e^2q_i^2n_e\ln\Lambda_{e,i}}{4\pi\varepsilon_0^2 m_i v_e} = f_{e,i}N_iJ_e\frac{eq_i^2\ln\Lambda_{e,i}}{4\pi\varepsilon_0^2 m_i v_e^2}. \tag{22}$$

Here, $\ln\Lambda_{e,i}$ is the Coulomb logarithm of species i due to collisions with electrons and v_e is the velocity of the beam electrons [see (29)]. The quantity $\Lambda_{e,i}$ is the ratio of the largest possible collision parameter (in a plasma the Debye length λ_d) to the mean collision parameter for 90° deflections during electron–ion collisions given by $\langle b_{90^\circ}\rangle_{e,i} = eq_i/8\pi\varepsilon_0 E_e$. This is a special case of the more general 90° deflection mean collision parameter for two charged species $\langle b_{90^\circ}\rangle_{i,j} = q_iq_j/8\pi\varepsilon_0 E_{\text{rel}}$ where E_{rel} is the relative energy of the two species. Since the ions in EBITs are actually unscreened the Debye length is to be replaced by the drift tube radius. $\Lambda_{e,i} = \ln(r_{dt}/\langle b_{90^\circ}\rangle)$ usually has a value of about 10. The heating is stronger for the more highly charged ions due to the q_i^2 dependence, so they are expected to be hotter.

Evaporative cooling occurs because the more energetic ions escape, leading to a net lowering of the ion temperature. As is shown in Fig. 6, this leads to significantly improved ion trapping. The energy lost due to the escape is given by [31]

$$\frac{3}{2}\frac{d}{dt}(N_ikT_i)^{Esc} = -N_i(q_iV_t + kT_i)R_i^{Esc}. \tag{23}$$

The results regarding escape, i.e., (15), (16), and (22), can be calculated invoking the Fokker–Planck equation. However, the distribution functions are actually non-Maxwellian because of the substantial losses for $v > v_{\text{thresh}}$, where v_{thresh} is the minimum velocity for ions of charge state q_i to escape from the trap axially. Nevertheless, if these losses occur far in the tail of the distribution functions, appropriate expressions are readily obtained [16]. Even for the case when the threshold velocity is approaching the thermal velocity analytic expressions have been derived from the Fokker–Planck equation [32].

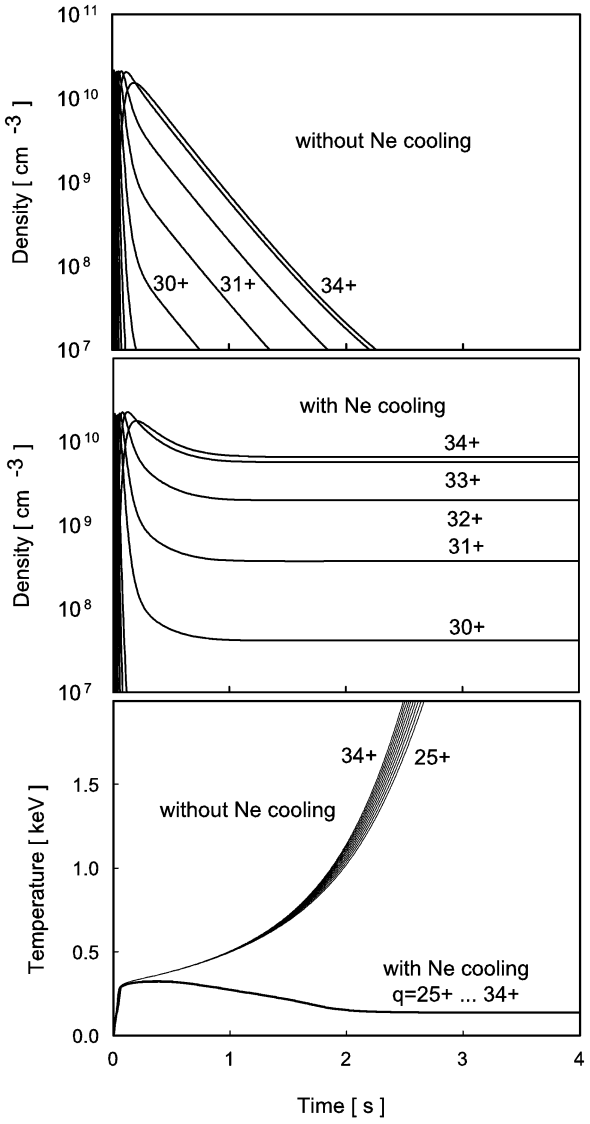

Fig. 6. Results of simulations of the density and temperature evolution of various Kr ions without and with continuous injection of neon. In the simulation, a puff of krypton was injected as a pulse of 1 ms duration. Beam current, $I_e = 100\ \text{mA}$, beam energy, $E_e = 10\ \text{keV}$, and axial potential, $V_t = 100\ \text{V}$ were constant throughout the simulations. Benefits of evaporative cooling are clearly demonstrated by the lower temperature and longer trapping times achieved when the neon is being injected.

Under most operating conditions, escape limits the equilibrium temperatures of the ions to typically 0.1–0.4 q_iV_t (i.e., $\omega_i \approx 2.5$ to 10). Lower charge states escape most easily, with the cooling effect being transferred to higher charge states through ion–ion collisions (i.e., ion–ion energy exchange). This process can be deliberately enhanced by introducing a light gas (typically Ne or N_2) which is rapidly ionized to its bare state when it acts to efficiently cool the more highly charged ions.

Ion–ion energy exchange occurs through collisions between the trapped ions. They interact via long range Coulomb forces.

The characteristic relaxation time for species i to interact with species j in this manner is given by [33]

$$\tau_{i,j} = \frac{3(2\pi)^{3/2}\epsilon_0 m_i m_j}{2q_i^2 q_j^2 n_j \ln\Lambda_{i,j}} \left(\frac{kT_i}{m_i} + \frac{kT_j}{m_j}\right)^{3/2} = 7.37\times 10^{12} \frac{\mu_i \mu_j}{\hat{q_i}^2 \hat{q_j}^2 n_j \ln\Lambda_{i,j}} \times \left(\frac{kT_i}{\mu_i} + \frac{kT_j}{\mu_j}\right)^{3/2} [s] \quad (24)$$

where the temperatures are in electronvolts, the density n_j in m^{-3}, and $\hat{q_i} = q_i/e$ and $\mu_i = m_i/m_u$ are charge and mass numbers and m_u is the unit atomic mass. Again, $\ln\Lambda_{i,j}$ is the ion–ion Coulomb logarithm. In an EBIS/T, scattering occurs by more than one type of ion so the appropriate frequencies $\tau_{i,j}^{-1}$ must be summed to give a characteristic frequency for the total collision of species i with all species. The $\hat{q_i}^2\hat{q_j}^2$ dependence in (24) shows the coupling between higher charge states is strongest (i.e., they have the shortest collision times). Accordingly, higher charge states tend to share energy most rapidly, having similar temperatures. The corresponding energy exchange among the ions is described by the expression

$$\frac{d}{dt}\left(\frac{3}{2}N_i k T_i\right)^{Exc} = N_i \sum_{j,\alpha} f_{i,j}\tau_{i,j}^{-1} k\left(T_j - T_i\right) \quad (25)$$

with $f_{i,j}$ being the ion–ion overlap factor. Again the summation is over the double index j, α to emphasize it is over all trapped ions. Finally, adding up the various terms given above we obtain a set of equations for the temperatures

$$\frac{d}{dt}\left(\frac{3}{2}N_i T_i\right) = \frac{d}{dt}\left(\frac{3}{2}N_i T_i\right)^{\mathrm{Beam}} + \frac{d}{dt}\left(\frac{3}{2}N_i T_i\right)^{\mathrm{Exc}} + \frac{d}{dt}\left(\frac{3}{2}N_i T_i\right)^{\mathrm{Esc}} \quad (26)$$

which is the energy equivalent to the particle balance (14). Note that the last two terms on the right hand side are again nonlinear, being similar to the last term in (14) in that they concern ion–ion collisions.

There are other less important phenomena including ionization heating, which can effect the energy dynamics of ions in an EBIS/T [17]. It can be shown that assuming ionization occurs uniformly across the electron beam then on average each ionizing event will result in an increase of the average energy of the ion of $V_0/2$ (or less if the depth of the radial well is reduced by ion compensation). Due to ion–ion collisions, this $V_0/2$, will be shared among the available degrees of freedom, as dictated by the principle of equipatition. For cold ions, motion occurs in a simple harmonic potential (since $\rho < r_e$), as given by (4) for the two coordinates perpendicular to the beam axis. This is analogous to an ion in a crystal lattice, so for each of these coordinates there are two degrees of freedom for energy storage, corresponding to equal amounts of potential and kinetic energy. In contrast, the axial potential is like a square-well (analogous to a gas atom in a box) so there is one degree of freedom, associated with the kinetic energy. These five degrees-of-freedom each store $\Delta kT/2$ of the energy. Hence, the average change in temperature due to each ionization event is given by $\Delta kT/2 = \Delta V/5 = V_0/10$ or $\Delta kT = V_0/5$, i.e., the initial temperature of ions would be about $q_i V_0/5$. Note this is per ion ionized, independently of how quickly the ionization occurs. Hence, this effect occurs even in the limit $t \to 0$ [34] and affects the ion temperature at very early times.

A closely related issue is the use of a square shaped axial trapping potential, as shown in Fig. 5. The more gently sloped the end potential walls are, then the greater the proportion of ions will be found along these regions of rising potential. This will result in a greater degree of ionizing heating (scaling with V_t not V_0) and hence hotter ions, lower electron–ion overlap factors, and lower ionization rates.

The work done expanding the ion cloud is an important but often neglected aspect of the energetics of ions in an EBIS/T. The average potential energy associated with ions of species i is given in dimensions of electronvolts by

$$\langle U_i\rangle = \frac{1}{N_i}\int_0^{r_{dt}} 2\pi\rho q_i V(\rho)\exp\left(-\frac{q_i V(\rho)}{kT_i}\right)d\rho. \quad (27)$$

When an ion cloud expands, work must be done as the ions climb up the potential. The heat capacity of ions of species i is given by

$$C_v = \frac{d\langle U_i\rangle}{dkT_i} + \frac{3}{2}. \quad (28)$$

It is useful to define a critical temperature T_c for ions to just leave the electron beam: $kT_c = q_i V_0$. This temperature then conveniently scales (28) for all species in the uncompensated limit (i.e., neglecting space charge of the ions). Fig. 7 shows the graph of C_v as a function of the scaled temperature, T/T_c. Numerical calculations which include the effect of compensation by the trapped ions show similar behavior as would be expected from asymptotic arguments about the form of this curve.

In the limit of low T/T_c, the ions have five degrees-of-freedom as discussed above. Hence in this asymptotic limit $C_v = 5/2$. In the limit of high T/T_c, the ions are no longer bound radially to the harmonic region given by (4) but are now also free to explore parts of potential given by (5). This means that the potential energy of the ion is no longer a degree of freedom in which energy can be stored and C_v takes on a value of 3/2 as is shown asymptotically in Fig. 7. In between these two limits, C_v can be seen to go through a maximum. The width and height of the maximum in the C_v curve are dependent on the distance at which the integral is truncated with the maximum becoming sharper and higher as this truncation distance is increased. All of this behavior is highly reminiscent of a phase transition. However, it is important to realize this is a second-order phase transition (i.e., one cannot identify the phase simply by looking at a small localized portion of the sample) in contrast to the more familiar first-order phase transitions (e.g., ice to water, where a microscopic sample is

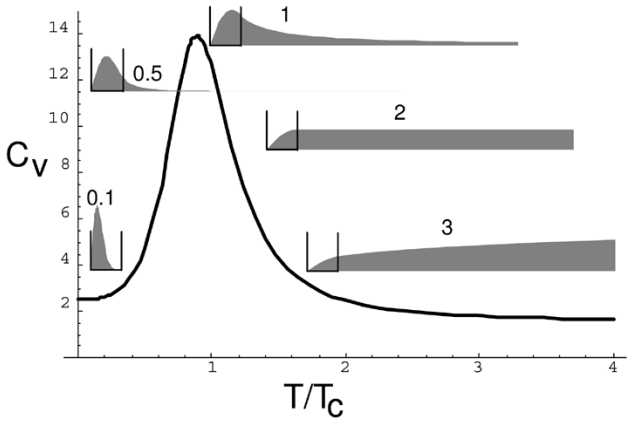

Fig. 7. C_v against normalized ion temperature T/T_c in the uncompensated limit (i.e., no ionic space charge). Heat capacity C_v was calculated by truncating the integrals implicit in (27) and (28) at 150 electron beam radii, an appropriate value for an EBIS/T corresponding to the typical drift tube radius. Calculated radial probability densities (i.e., probability of finding a given ion at a given radius from the electron beam) are shown as shaded distributions for different temperatures. In each case, the distribution is labeled with the corresponding temperature in units of T_c. Horizontal axis for these distributions goes out to 10 electron beam radii with the vertical lines denoting the portion inside the electron beam. Hence, the area inside the thin line compared to the total area is the electron ion overlap factor.

sufficient to determine the phase). Furthermore, this is a phase transition involving the electron beam and the trapped ions as a system and not just the trapped ions. This type of phase transition should not be confused with formation of Coulomb crystals, a first-order phase transition among ions alone.

The existence of the maximum in Fig. 7 indicates that it is hard to drive the ions radially away from the electron beam and hence points directly to the basic means of ion trapping in EBIS/Ts. In a very interesting experiment involving imaging the ion cloud Porto *et al.* [35] reported that they were unable to create ion distributions characteristic of $T/T_c > 1$. With considerable effort, by carefully adjusting the trap parameters, Kinugawa *et al.* [36] were able to access this region and then drive the ions back through the phase transition with the result being a sudden burst of X-ray radiation due to the ions collapsing back into the electron beam along with cooling from axial escape.

The difficulty encountered in forming stable ion distributions with $T/T_c > 1$ can be appreciated through examination of the radial probability distributions. It is hard to drive the ions past the region $T/T_c > 1$ because of the increasing heat capacity. However, when one does, if the system is driven too hard, the distribution will extend out to the drift tube walls, leading to considerable radial escape. Indeed, above a value of $T/T_c = 2$, the distribution can no longer be normalized, meaning the ions are no longer bound to the electron beam at all.

In summary, the dominant effects in determining the temperature dynamics of the ions are electron beam heating (mostly of the higher charge states) balanced by cooling due to axial escape (mostly of the lower charge states). Ion–ion energy exchange transfers energy from the more highly charged ions down to the less highly charged ones. Since ion–ion energy exchange occurs most efficiently between high charge states (frequency proportional to $q_i^2 q_j^2$), the difference in temperature between neighboring charge states is expected to decrease as the charge increases. At short times after trapping is started, ionization heating can play a role, leading to an initial ion temperature of about $q_i V_0/5$.

E. Upper Bound on EBIS/T Performance

There have been various attempts to model EBIS/T performance over the years [37], [38] and this effort continues [28], [32]. For injection of a single element for which E_e is sufficiently high to create ions of charge state $q_i = i \times e$, simulations require the solution of $2(i+1)$ differential equations. $i+1$ of these differential equations take the form of (14), representing the densities of the different charge states present.

Another $i+1$ differential equations represent the temperatures of these charge states, taking account of the various processes described in Section II-D, representing each of the energy-changing effects as a term in a differential equation. If two elements are being injected into the EBIT, then the number of equations increases accordingly. The solution of these coupled differential equations is a time consuming task, requiring the use of a powerful computer. It is useful to develop a simpler description from which approximate estimates of what an EBIS/T's performance can be calculated. Such an estimate can be arrived at by assuming that the electron beam's space charge is fully neutralized in a time t_i^{app} as given by (18).

The total number of electrons in the trap at any time is given by $I_e l/(ev_e)$ where e is the electron charge, I_e is the total beam current, l is the trap length, and v_e is the velocity of electrons in the beam, given by

$$v_e \approx c\sqrt{1-\left(\frac{E_e[\mathrm{keV}]}{511}+1\right)^{-2}} \tag{29}$$

with $c \approx 3\times 10^8\,\mathrm{m/s}$. Assuming the electron beam is fully compensated by a single trapped species of charge number $\hat{q}$, there will be a factor of $\hat{q}$ less trapped ions. For multiple charge states, $\hat{q}$ is simply interpreted as the average charge number present.

With this assumption, after t_i^{app}, the number of ions in the trap, of length l will be $I_e l/(qv_e)$. Consider that after this time, all of these ions are then delivered to another apparatus by emptying the trap. It must be stressed that this is an overestimate but at least it provides an upper bound on the rate of ion delivery in terms of a few machine parameters. Combining this equation with (3) and (18) and making suitable conversion of units, one arrives at the result for the rate at which ions of charge $\hat{q}_i = q_i/e$ can be created as

$$\begin{aligned} R_i \approx \frac{N_i}{t_i^{\mathrm{app}}} &= \frac{I_e^2 lB}{2\sqrt{2}e^2\pi r_c v_e \sqrt{\frac{mkT_c}{e^2}}\hat{q}_i \sum_{j=0}^{\hat{q}_i}\frac{1}{\sigma_j^{EI}}} \\ &\approx 1.84\times 10^{42}\frac{I_e^2 lB}{r_c v_e \sqrt{kT_c}\hat{q}_i \sum_{j=0}^{\hat{q}_i}\frac{1}{\sigma_j^{EI}}}\left[\frac{\mathrm{ions}}{s}\right] \end{aligned} \tag{30}$$

where kT_c is in electronvolts and all other quantities in SI-units. For a typical set of parameters ($I_e = 0.1\,\mathrm{A}, l = 1\,\mathrm{cm}, B = 3\,\mathrm{T}$, $kT_c = 0.1\,\mathrm{eV}$, $r_c = 1\,\mathrm{mm}$, $E_e = 10\,\mathrm{keV}$) we estimate from

(30) a production rate of Kr^{33+} ions of $R_i \approx 2 \times 10^7\ s^{-1}$ (with $\sum_{j=0}^{33} 1/\sigma_j^{EI} \approx 3 \times 10^{25}\ m^{-2}$).

The cross sections $\sigma_i^{EI}(E_e)$ can usually be evaluated to sufficient precision using for example the well-known Lotz formula [39], with a relativistic correction applied [40] where appropriate. All of the remaining factors in this equation are directly determined from a given EBIS/Ts design and operating parameters, the charge state required and e, the elementary charge.

It must be emphasized that (30) provides an overestimate of the creation rate for several reasons. In practice, the electron beam's space charge cannot be neutralized or trapping will no longer occur. In any case, before this happens, a significant fraction of the ions will be outside the electron beam as its trapping potential progressively weakens due to compensation. Furthermore, it takes longer than t_i^{app} for significant compensation to occur.

F. Ion Extraction

Ions can leave the trap along the beam axis traveling toward the collector by passing over the potential barrier provided by the final drift tube. The horn shape of the final drift tube (see Fig. 5) is fashioned so that once over the maximum in the potential barrier, the space charge potential gently accelerates the ions further along the beam axis and out of the trap region. Once out of the trap region, these ions are quickly accelerated along the beam axis toward the collector. Some of these ions pass through the collector assembly, including a final extractor electrode to enter a beam optics system. The exact nature of this beam optics depends on the particular application but usually includes a charge selection magnet (Wien filter) so that a single charge state can be selected for subsequent use.

There are various extraction modes possible, depending on the voltage waveforms applied to the drift tube system. The simplest to implement is *leaky mode* extraction where ions escape axially as described in Section II-D. As described previously, when working in this mode, it is usual to configure the trap asymmetrically so ions escape moving toward the collector as desired.

Pulses of ions can be extracted (*pulsed mode*), by either raising the potential of the central drift-tube above that of the two end drift tubes or by lowering the potential of the final drift tube, with either change occurring typically in a few milliseconds. Although the two pulsed expulsion methods are similar, raising the potential of the central drift-tube has the advantage that the ions all leave the trap from the same potential throughout the extraction process and hence are equally well matched to the ion optics. Essentially, the time-varying potential applied to the central drift tube acts as a potential elevator for the colder ions. Leaky mode tends to be less effective at extracting the highest charge states trapped as they have lower escape rates. However, the energy distribution of the leaky mode ions is narrower.

If one considers pulsed mode extraction with a period of t_i^{app}, the rate of delivery into an experiment might be considered to be that given by (30). It is important to note that the extraction efficiency is typically 10% or less. That is to say that the majority of the ions leaving the trap are lost (usually in the collector) rather than being successfully delivered into the subsequent apparatus. Just as the electron beam expands as the magnetic field reduces from the trap region toward the collector, so too does the extracted ions beam, with many of the ions hitting the electrodes in the collector structure. The greater the ion temperature, the greater is this expansion so the extraction efficiency tend to fall as the ion temperature rises. Finally, in general, several charge states will be present in the trap so if a single charge state is then selected, the ion yield will again fall. Typically, in practice, the rate of ion delivery from an EBIS/T is one or two orders of magnitude less than that estimated from (30).

In some applications, there are specific timing requirements whereby the ions must be delivered in short pulse length bunches due to the demands of the system being served by the EBIS/T. An example of this requirement is single turn injection into a synchrotron for hadron therapy [41] where pulse times of the order of 1 μs are required. To achieve such short pulse times, the drift tubes can be carefully fashioned to interpenetrate each other. Then, when set to the voltages required to extract the ions, a smooth linear potential gradient is created rather than a staircase, negating the effect of the increased space charge of the uncompensated electron beam acting behind the ion cloud as it is extracted from the trap. Combining this particular drift tube structure with appropriate, fast rise time waveforms applied, one to each drift tube results in complete extraction of the ions on a microsecond time scale as required [41].

In contrast, in the *pulsed evaporative cooling* scheme [36], the electrostatic trap potential is gradually reduced so hotter ions are sacrificially evaporated leading to cooling (see Section II-D) and contraction of the ion cloud (see Section II-B). Toward the end of this extraction process, ions leaving the trap have a very narrow energy spread whilst retaining the higher charge states in the extracted ion distribution. This narrow energy spread is ideal for efficient ion extraction although the pulse length of the extracted ions must be long, rendering this technique unsuitable for many applications.

III. Experiments Related to Machine Physics

A. Measured Charge Balance Dynamics

It is possible to measure the charge balance dynamics in two distinct ways. One can start with an open trap, close it and extract ions after a given *cooking time*. Passing these ions through a charge separating magnet and onto a detector, one can measure the yield of a given charge state. By changing the cooking time systematically, the charge balance as a function of time can be determined.

Fig. 8 shows an example of such a measurement. Notice that in between the peaks due to dumping of the ions, there is a slowly rising rate of ion detection due to the ions which are escaping from the trap. This is indicative that the temperature of the ions is changing along with the charge balance. The extraction efficiency is a function of the ion temperature so it is difficult to directly infer the charge balance dynamics from such data although it can provide a rough guide of the charge balance dynamics. However, as is discussed in Section III-B, comparison between the yield of escaping ions and dumped ions can be used to infer the temperature from such data.

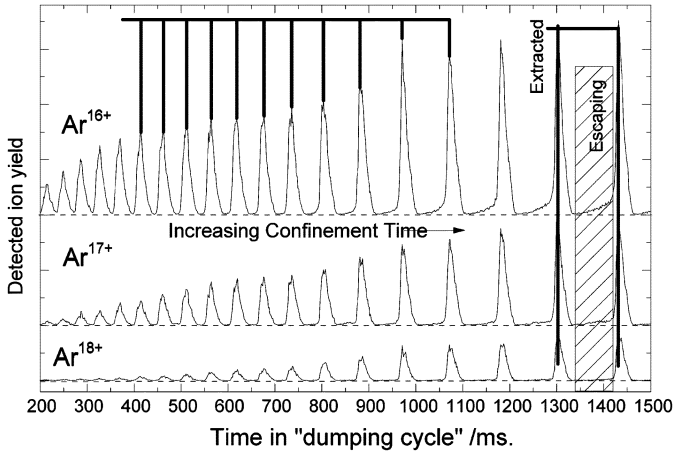

Fig. 8. Measured yields of Ar^{16+}, Ar^{17+}, and Ar^{18+} through a cycle of lengthening cooking times. Apart from the changing of the central drift tube potential to dump the ions, the machine parameters were kept constant with values of $E_e = 20\,\mathrm{keV}$, $I_e = 60\,\mathrm{mA}$, $B = 4\,\mathrm{T}$. During the cooking periods, a 10 V difference was applied to the final drift tube with respect to the central, corresponding to $V_t \approx 16\,\mathrm{V}$.

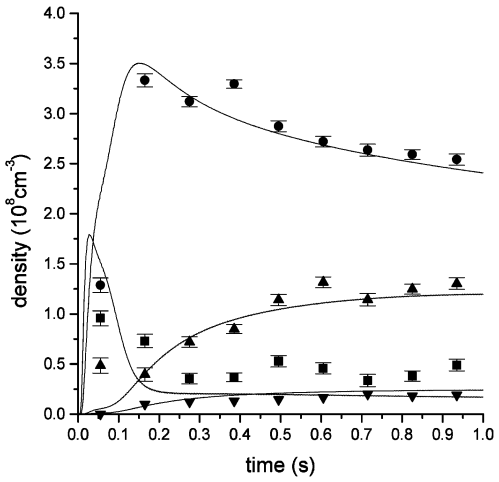

Fig. 9. Measured densities of Ti^{19+} (squares), Ti^{20+} (circles), Ti^{21+} (triangles) and Ti^{22+} (inverted triangles) as a function of time since injection compared to a simulation of the same. Conditions assumed for the simulation match those of the experiment and are $B = 4.0\,\mathrm{T}$, $r_e = 30\,\mu\mathrm{m}$, $I_e = 50\,\mathrm{mA}$, initial Ti^{+} density $= 4.0 \times 10^8\,\mathrm{cm}^{-3}$, constant Ne neutral density $= 2.0 \times 10^9\,\mathrm{cm}^{-3}$. Beam energy was scanned from 11 to 3 kV, then from 3 to 11 kV, within a period of 4 ms [28].

A more useful diagnostic of charge balance dynamics can be made through measurement of characteristic photons which leave the trap region of an EBIT. Fig. 9 shows the results of analysing the time dependence of such characteristic photons during an experiment where the beam energy was being rapidly swept with a triangular waveform across a group of dielectronic recombination resonances. This data is rich in physical information and can be analyzed to determine the resonance strengths of some of these resonances [42]. This data also contains characteristic signals related to different charge states of the trapped ions from which the number of ions inside the electron beam can be determined. It is important to note that these density determinations are independent of the electron beam radius and give the average density across the electron beam.

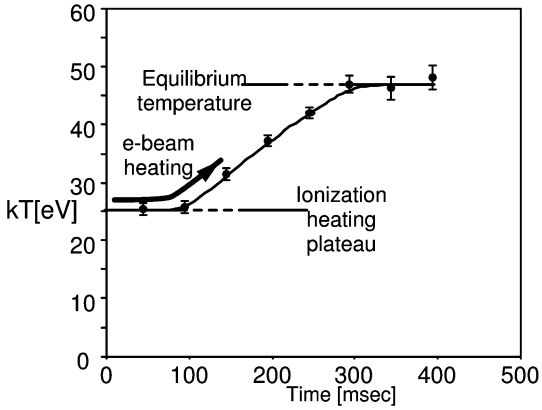

Fig. 10. Measured temperature of Ar^{17+} and Ar^{18+} ions as a function of time after the trap was closed (i.e., ion creation initiated). Conditions are the same as those given in Fig. 8.

Fig. 9 shows the results of such a measurement and comparison with simulation. The hydrogen-like Ti^{21+} density was inferred from the radiative recombination signal which occurs at all electron beam energies. The helium-like Ti^{20+} density was inferred from the KLL (i.e. one electron has been removed from the K shell with it and a new electron each populating the L shell) dielectronic recombination resonance which is clearly resolved from the same resonance occurring in other charge states. Similarly, the lithium-like Ti^{19+} density was inferred from the KLM (one electron has been removed from the K shell with it and a new electron, one in each, populating the L and M shells) dielectronic recombination resonance. Since the cross section (or resonance strength) is well known for each of these processes and total detection efficiency of the system can be determined from geometrical factors and known window absorptions, it is possible to convert detected photon rates into absolute densities of trapped ions for each of these characteristic signals.

The beam energy is swept so that rapidly, for each period of the beam energy waveform the charge balance can be considered constant. The comparison to these measurements was made in the framework described in Section II. However, the presence of the dielectronic recombination resonances acts to increase the recombination rate. This can be accounted for in (14) by replacing σ_i^{RR} with the correctly weighted average of the dielectronic and radiative recombination cross sections. Indeed, if this is not done, there is not such good agreement between the measured and simulated charge balance dynamics [28].

In making such comparisons, there is considerable uncertainty regarding the initially injected densities. In practice the initial Ti^{+} density is adjusted to match the final observed ion densities while the simulations are fairly insensitive to the constant neutral density.

B. Temperature Dynamics

As described in (15) and (16), the axial escape rate is a function of the temperature of the ions. By comparing the relative numbers of dumped and escaping ions for two adjacent (high) charge states as a function of time, it is possible to track the temperature dynamics. Fig. 10 shows the results of such an analysis. In the limit $t \to 0$, the measured temperature is not zero, because of ionization heating [34]. Using the machine parameters, this

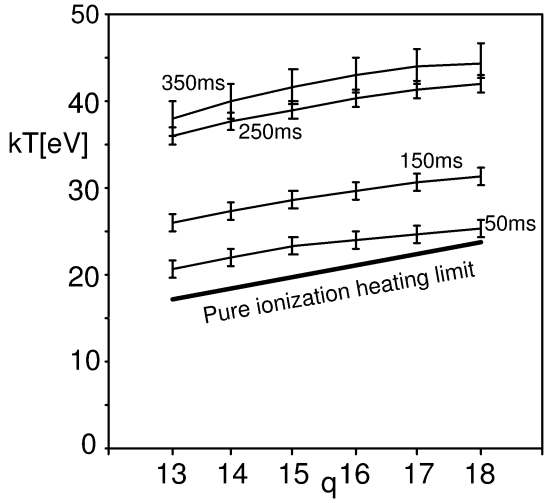

Fig. 11. Measured temperature distribution of Ar ions as a function of time after the trap was closed (i.e., ion creation initiated). Conditions are the same as those given in Fig. 8.

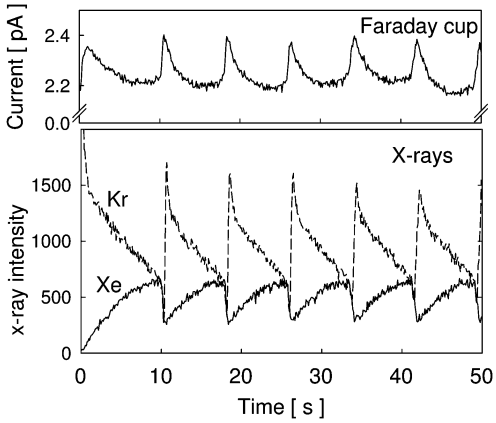

Fig. 12. Upper plot: Measured current of ions expelled from the trap in axial direction. Lower plot: Corresponding time profile of $n = 2 - 1$ and $n = 3 - 2$ emission spectra of Kr and Xe ions. Fixed parameters: $E_e = 5\ \mathrm{keV}$, $V_t = 10\ \mathrm{V}$, pressure ratio: $p_{\mathrm{Kr}}/p_{\mathrm{Xe}} = 85.0$ (reproduced with permission [32]).

temperature is predicted to be 23 eV from the ionization heating analysis $kT(t \rightarrow 0) = q_i V_0/5$, as described in Section II-D. This is in good agreement with the observation. The temperature of the ions subsequently increases due to electron beam heating until it eventually attains an equilibrium value, again as predicted by the machine physics outlined in Section II.

By further modeling the temperature as a quadratic function of charge state, the full temperature dynamics of the trapped ions can be recovered [34], as shown in Fig. 11. Temperatures increase with both time and with charge state as expected. Also, the increase with charge state becomes less for higher charge states, again as predicted.

C. Sawtooth Oscillations

Although the comparisons between the predicted and measured machine physics outlined above give confidence on the general model, the phenomena all happen on relatively long time scales. Furthermore, none of the phenomena observed can in any sense be described as a surprise. The true value of any predictive model is that it can account for observations which were not previously expected. One such phenomenon is sawtooth oscillations observed in EBIS/Ts.

The characteristic times for establishing ionization equilibrium in an EBIS/T is of the order of 0.1–1 s. For a long time, it was the common opinion that on this scale, any relaxation to a new stationary state should occur. It was, therefore, a great surprise when sawtooth like instabilities with periodic intervals of several seconds were observed for the first time in the Berlin EBIT [43]. Such effects do occur when, in addition to a heavy component, a light element is injected into the trap for cooling purposes. As has already been mentioned, this evaporative cooling is essential for the production and storage of very highly charged ions. A substantial prerequisite for the creation of sawtooth oscillations is that the commonly applied conditions for the cooling technique are changed: the rate at which the light element (coolant gas) is added to the trap is much larger than the influx of the heavy component. Because of the low influx of the heavy atoms, they concentrate in the trap during an extended accumulation period (several seconds) until the cooling from the (decreased) low-Z ions is no longer sufficient and a sudden collapse of the ion population occurs.

Whereas first measurements [31], [43] were carried out for a mixture of argon and barium ions, in more recent studies [32], a continuous flow of xenon $(Z = 54)$ atoms is mixed with argon $(Z = 18)$ or krypton $(Z = 36)$ as a coolant. Fig. 12 shows an example for the Xe–Kr combination. The EBIT was operated in a static mode where all experimental parameters (applied voltages, beam current, magnetic field strength, gas flow) were kept constant. The electron-beam energy was fixed at $E_e = 5\ \mathrm{keV}$, limiting the ionization to the maximum charge state of Kr to $34+$, and Xe to $44+$. Characteristic X-ray spectra of the confined ions were measured in the range 500 eV to 15 keV using a solid-state Ge detector. The pulse-height information of the X-ray energy was digitized by an analog-to-digital converter (ADC) and counted by a multichannel scaler as a function of time. In the lower part of Fig. 12, time traces representative for Kr and Xe ion concentrations are shown by the X-ray intensity for $n = 2 - 1$ and $n = 3 - 2$ transitions.

The prominent sawtooth structure of the X-ray emission is clear evidence that the population in the trap does not reach a steady state. The signal for Kr (Xe) ions decreases (increases) steadily over successive time periods of about 8 s. Toward the end of each period, a sudden drop in the intensity is observed in the radiation, indicating rapid ion expulsion from the trap. The particles are mainly lost parallel to the beam axis as is demonstrated by the measured current trace in Fig. 12 (top). This current was measured by capturing the escaping ions in a Faraday cap at the end of the EBIT. There is always a drastic reduction of the inventory of the cooling ions (Kr) at the final crash of each sawtooth while the loss of the high Z-component (Xe) is much less pronounced. This difference in behavior of ion expulsion is indicative for a strong outflow of energy transferred from the higher charge state Xe ions to the Kr ions leaving the trap.

In an extended parameter study, the beam current $(I_e = 50\text{–}120\ \mathrm{mA})$, axial voltage trap potential $(V_t = 3\text{–}46\ \mathrm{V})$ and the magnetic field strength $(B = 2.4\text{–}2.8\ \mathrm{T})$ were varied to find out under which conditions sawtooth behavior occurs. It

was found that for each parameter the sawtooth phenomenon exists only within well defined windows. As a striking example, it is observed that in a Xe-Ar mixture, a repetition time of 5 s is found for $I_e = 100$ mA. However, increasing the current marginally to 102 mA, there is just one single crash at the beginning; thereafter, the system is in a completely stationary mode. Clearly, this phenomenon is very sensitive to the machine parameters and as such it is an excellent benchmark of the proper description of EBIS/T machine physics.

It is encouraging that the sawtooth phenomenon is observed in at least two independent implementations of models of the machine physics of EBIS/Ts [28], [32] constructed broadly along the lines outlined in Section II. However, the agreement is still at the phenomenological level. The exact ranges of parameters over which the phenomenon is observed, the period and depth of the sawtooth have not yet been shown to be in good agreement. Current activity is directed toward improving the machine physics to give better agreement with the observed sawtooth data. It is worth noting that it is very hard to ascertain the true neutral density in the trap, which is one of the parameters the sawtooth phenomenon is sensitive to.

From a mathematical point of view, the sawtooth events are assigned to a Hopf-bifurcation: the system bounces between two extreme states. Physically, their occurrence may be explained along the following line using the xenon–argon system as an example: Xe ions accumulate in the trap at low temperature. They are cooled by the Ar ions which in turn escape from the trap more rapidly because of their lower charge. Ar-ions are thus continuously replaced by Xe-ions. This process continues until the cooling capability is considerably reduced because of insufficient Ar density. As a consequence, the ion temperatures rise substantially thereby enhancing the particles losses further. In particular, the lower charge state Ar ions are confined less well in the trapping potential and are almost completely lost by axial escape. The production of Ar-ions in the higher charge state via ionization is thereby also effectively suppressed. Xe ions are also driven out from the trap but to a lesser extent. Once their density is markedly decreased, the rate at which energy is transferred to the Ar ions slows down. This allows fresh Ar ions to populate the trap and stay longer in the electron beam. The ions are confined at the low initial temperature and concentrate in the trap until their density becomes sufficiently high that the competition between Ar and Xe starts again.

IV. Conclusion

The general form of EBIS/Ts has been described briefly with the various constituent parts being described in turn. Following this, the machine physics underlying EBIS/Ts has been discussed with reference to a wide range of atomic and plasma physics processes which occur inside the trap. Some diagnostic measurements have been presented which broadly support this model of the machine physics. In particular, the importance of proper understanding of the energetics of the trapped ions and the importance of the sawtooth phenomenon have been emphasized. The range of machines in operation or currently under development (see for example, [13]) indicates that this is a lively and ongoing field.

Acknowledgment

The authors are deeply indebted to many members of the EBIS/T-users community with whom they have had fruitful discussions over many years which have influenced the contents of this paper. In particular, R. Becker, C. Biedermann, J. Gillapsy, T. Kinugawa, X. Lu, N. Nakamura, K. Okuno, S. Ohtani, R. Radtke, and H. Watanabe are acknowledged in this respect.

References

[1] E. D. Donets and V. P. Ovsyannikov, "Investigation of ionization of positive ions by electron impact," *Sov. Phys. JETP*, vol. 53, pp. 466–466, 1981.

[2] E. D. Donets, V. I. Ilushenko, and V. A. Alpert, "Ultrahigh vacuum electron beam ion source of highly stripped ions," in *Proc. 1st Int. Conf. Ion Sources*, Saclay, France, 1969, pp. 635–635.

[3] W. Bleakney, "A new method of positive ray analysis and its application to the measurement of ionization potentials in mercury vapor," *Phys. Rev.*, vol. 34, pp. 157–157, 1929.

[4] R. H. Plumlee, "Space charge neutralization in the ionizing beam of a mass spectrometer," *Rev. Sci. Instrum.*, vol. 28, pp. 830–830, 1957.

[5] F. A. Baker and J. B. Hasted, "Electron collision studies with trapped positive ions," *Proc. R. Soc. A*, vol. 261, pp. 33–33, 1966.

[6] P. A. Redhead, "Multiple ionization of the rare gases by successive electron impacts (0–250 eV). I. Appearance potentials and metastable ion formation," *Can. J. Phys.*, vol. 45, pp. 1791–1791, 1967.

[7] R. W. Schmieder, C. L. Bisson, S. Haney, N. Toly, A. R. Van Hook, and J. Weeks, "Sandia super-EBIS," *Rev. Sci. Instrum.* , vol. 61, pp. 259–259, 1990.

[8] M. A. Levine, R. E. Marrs, J. R. Henderson, D. A. Knapp, and M. B. Schneider, "The electron beam ion trap: A new instrument for atomic physics measurements," *Phys. Scr.*, vol. T22, pp. 157–157, 1988.

[9] M. A. Levine, R. E. Marrs, and R. W. Schmieder, "Measurements of instabilities and ion heating in an electron beam ion source," *Nucl. Instrum. Meth.*, vol. A237, pp. 429–429, 1985.

[10] J. R. Crespo *et al.*, "Progress at the Heidelberg EBIT," in *J. Phys.*, vol. 2, 2004, pp. 52–52.

[11] D. A. Knapp, R. E. Marrs, S. R. Elliot, E. W. Magee, and R. Zasadinski, "A high-energy electron beam ion trap for production of high-charge high-Z-ions," *Nucl. Instrum. Methods Phys. Res. A*, vol. 334, pp. 305–305, 1993.

[12] R. E. Marrs, S. R. Elliot, and D. A. Knapp, "Production and trapping of hydrogen-like and bare uranium ions in an electron beam ion trap," *Phys. Rev. Lett.*, vol. 72, pp. 4082–4082, 1994.

[13] "Proceedings of the ninth international symposium on electron beam ion sources and traps and their applications," *J. Phys.*, vol. 2, pp. 1–220, 2004.

[14] T. A. Carlson, C. W. Nestor, N. Wasserman, and J. D. McDowell, "Calculated ionization potentials for multiply charged ions," *At. Data*, vol. 2, pp. 63–63, 1970.

[15] F. J. Currell, "The physics of electron beam ions traps," in *Trapping Highly Charged Ions: Fundamentals and Applications*, J. Gillaspy, Ed. New York: Nova, 1999, sec. 5.

[16] G. Fussmann, C. Biedermann, and R. Radtke, "EBIT: An electron beam source for the production and confinement of highly ionized atoms," in *Advanced Technologies Based on Wave and Beam Generated Plasmas*, H. Schlüter and A. Shivarova, Eds. Dordrecht, Germany: Kluwer, 1999, pp. 429–429.

[17] F. J. Currell, "Electron beam ion traps and their use in the study of highly charged ions," in *The Physics of Multiply and Highly Charged Ions*, F. J. Currell, Ed. Dordrecht, Germany: Kluwer, 2003, vol. 1, Sources, Applications and Fundamental Processes.

[18] R. Becker and W. B. Herrmannsfeldt, "The design of electron and ion guns, beams and collectors," in *J. Phys.*, vol. 2, 2004, pp. 52–52.

[19] . Field Precision, Albuquerque, NM. [Online]. Available: http://www.fieldp.com

[20] G. J. Herrmann, "Optical theory of thermal velocity effects in cylindrical electron beams," *Appl. Phys.*, vol. 29, pp. 127–127, 1958.

[21] M. A. Levine, R. E. Marrs, J. N. Bardsley, P. Beiersdorfer, C. L. Bennet, M. H. Chen, T. Cowan, D. Dietrich, J. R. Henderson, D. A. Knapp, A. Osterheld, B. M. Penetrante, M. B. Schneider, and J. H. Schofield, "The use of an electron beam ion trap in the study of highly charged ions," *Nucl. Instrum. Meth.*, vol. B43, pp. 431–431, 1989.

[22] "EBIT Electron Beam Ion Trap, N-Div. Exp. Phys. Bi-Annu. Rep. 1996–1997," Lawrence Livermore Nat. Lab., Livermore, CA, 1998.
[23] H. Kuramoto, T. Kinugawa, H. Watanabe, C. Yamada, S. Ohtani, I. Yamada, and F. J. Currell, "Thomson scattering system at the Tokyo electron beam ion trap," *Rev. Sci. Instrum.*, vol. 73, pp. 42–42, 2002.
[24] R. E. Marrs, S. R. Elliot, and J. H. Schofield, "Measurement of electron-impact ionization cross sections for hydrogenlike high-Z ions," *Phys. Rev. A, Gen. Phys.*, vol. 56, pp. 1338–1338, 1997.
[25] B. E. O'Rourke, H. Watanabe, and F. J. Currell, "Electron impact ionization of hydrogen-like ions," in *The Physics of Multiply and Highly Charged Ions*, F. J. Currell, Ed. Dordrecht, Germany: Kluwer, 2003, vol. 1, Sources, Applications and Fundamental Processes.
[26] H. Watanabe, B. O'Rourke, F. J. Currell, S. Ohtani, and X. M. Tong, "Electron impact ionization of hydrogen-like molybdenum ions," *J. Phys. B At. Mol. Opt. Phys.*, vol. 35, pp. 5095–5095, 2002.
[27] V. P. Pastukhov, "Collisional losses of electrons from an adiabatic trap in a plasma with a positive potential," *Nucl. Fusion*, vol. 14, pp. 3–3, 1974.
[28] X. Lu, "Systems to study collisions of electrons and highly charged ions," Ph.D. dissertation, Queen's Univ., Belfast, U.K., 2005.
[29] P. Beiersdorfer, L. Schweikhard, J. C. López-Urrutia, and K. Widmann, "X-ray emission following low-energy charge exchange collisions of highly charged ions," *Rev. Sci. Instrum.*, vol. 67, pp. 3818–3818, 1996.
[30] C. L. Longmire and M. N. Rosenbluth, "Diffusion of charged particles across a magnetic field," *Phys. Rev.*, vol. 103, pp. 507–507, 1957.
[31] R. Radtke, C. Biedermann, and P. Bachmann, "Sawtooth-like X-ray emission observed in EBIT," *Nucl. Instrum. Meth.*, vol. B205, pp. 250–250, 2003.
[32] R. Radtke, C. Biedermann, P. Bachmann, G. Fussmann, and T. Windisch, "Sawtooth oscillations in EBIT," in *J. Phys.*, vol. 2, 2004, p. 84.
[33] L. Spitzer Jr, *Physics of Fully Ionized Gases*. New York: Interscience, 1956.
[34] F. J. Currell, H. Kuramoto, S. Ohtani, C. Scullion, E. J. Sokell, and H. Watanabe, "Measurements of the temperature dynamics of ions trapped inside and electron beam ion trap and evidence for ionization heating," *Phys. Scr.*, vol. T92, pp. 147–147, 2001.
[35] J. V. Porto, I. Kink, and J. G. Gillaspy, "Direct imaging of highly charged ions in an electron beam ion trap," *Rev. Sci. Instrum.*, vol. 71, pp. 3050–3050, 2000.
[36] T. Kinugawa, F. J. Currell, and S. Ohtani, "Use of 'bursting evaporation' to cause a drastic contraction of the ion cloud in an electron beam ion trap: Transition into a high-density phase of cold, trapped highly charged ions," *Phys. Scr.*, vol. T92, pp. 102–102, 2001.
[37] B. M. Penetrante, J. N. Bardsley, D. DeWitt, M. W. Clark, and D. Schneider, "Evolution of ion-charge-state distributions in an electron-beam ion trap," *Phys. Rev. A, Gen. Phys.*, vol. 43, pp. 4861–4861, 1991.
[38] "Studies of highly ionized atoms using an electron beam ion trap," Ph.D. dissertation, H. S. Margolis, Pembroke College, Oxford, U.K., 1994.
[39] W. Lotz, "Electron-impact ionization cross-sections and ionization rate coefficients for atoms and ions from hydrogen to calcium," *Z. Phys*, vol. 216, pp. 241–241, 1968.
[40] M. Gryzinski, "Two-particle collisions. II. Coulomb collisions in the laboratory system of coordinates," *Phys. Rev.*, vol. 138, pp. A322–A322, 1965.
[41] H. Höltermann, R. Becker, M. Kleinod, and I. Müller, "Fast ion extraction for the medebis," in *J. Phys.*, vol. 2, 2004, pp. 94–94.
[42] B. E. O'Rourke, H. Kuramoto, Y. M. Li, S. Ohtani, X. M. Tong, H. Watanabe, and F. J. Currell, "Dielectronic recombination in He-like titanium ions," *J.Phys. B*, vol. 37, pp. 2345–2345, 2004.
[43] R. Radtke and C. Biedermann, "Sawtooth activity of the ion cloud in an electron-beam ion trap," *Phys. Rev. A, Gen. Phys.*, vol. 67, pp. 032 705–032 705, 2003.

Fred Currell was born in Welwyn Garden City, U.K., in 1963. He received the B.Sc. Hons. degree in physics and chemistry and the Ph.D. degree in atomic physics from the Manchester University, Manchester, U.K., in 1984 and 1987, respectively.

During 1994–1999, he was a Lecturer and the rose to Associate Professor at the Institute for Laser Science, University of Electrocommunications, Tokyo, Japan. Since 1999, he has been with the School of Mathematics and Physics, Queen's University, Belfast, U.K., as a Lecturer and then rose to Reader. Since 2004, he has also served as the Head of Department Physics Astronomy, Queen's University. He is a member of the International Advisory Board for the Highly Charged Ion Conference (since 2001) and for the Electron Beam Ion Source and Trap Conference (since 2004). He was the inventor of "Planar electrode arrays for charged particle trapping and manipulation," PCT/GB2003/003 683.

Gerd Fussmann was born in Velbert, Germany, in 1942. He studied physics at universities in Darmstadt and Bochum, Germany. He received the diploma and doctorate from Ruhr-University, Bochum, Germany, in 1974.

He has held the following positions: member of the Scientific Staff of Institut fur Plasmaphysik (IPP), Garching, Germany (1975–1992); guest stay JET, Culham, U.K. (1987); lectures and Habilitation at Augsburg University, Augsburg, Germany; Full Professor (Plasma Physics) at the Humboldt-Universität, Berlin, Germany. He has been a Director and Scientific Member of the Max-Planck Society. He has been a Member of the Scientific Board of the Max Planck Institute for Plasma Physics since 1993. He is a co-editor of the magazine *Contributions to Plasma Physics*. He has been a Speaker of the DFG-Board on Optics, Molecules, Atoms and Plasmas since 2004.